ACTA ONCOLOGICA
2023, VOL. 62, NO. 11, 1389–1393
https://doi.org/10.1080/0284186X.2023.2249221

Taylor & Francis
Taylor & Francis Group

LETTER TO THE EDITOR

Biologically guided automated treatment planning and evaluation: potential for treatment adaptation in head and neck cancer

Ana Ureba[a,b], Iuliana Toma-Dasu[a,b] and Marta Lazzeroni[a,b]

[a]Department of Physics, Medical Radiation Physics, Stockholms Universitet, Stockholm, Sweden; [b]Department of Oncology-Pathology, Medical Radiation Physics, Karolinska Institutet, Stockholm, Sweden

ARTICLE HISTORY Received 23 May 2023; Accepted 8 August 2023

Introduction

Radiation therapy is among the main treatment options offered as a non-surgical solution in the treatment of cancer. This technology-driven treatment modality has evolved significantly over the past few decades, aiming to improve the therapeutic ratio and local tumour control. Modern external beam radiotherapy such as intensity modulated radiotherapy (IMRT), intensity modulated arc therapy (IMAT) or volumetric arc therapy (VMAT), and intensity modulated proton therapy (IMPT) approaches modulate intensity to deliver precisely the radiation doses required to specific areas within the tumour, and to spare nearby organs [1,2]. The use of these techniques in combination with image-guided techniques and multimodality imaging has provided more accurate radiotherapy allowing for a reduction of long-term adverse effects [3]. Nowadays, most treatment planning systems (TPS) integrate imaging information for the diagnosis, planning, and delivery process, offering tools for image registration and fusion, dose calculation, and optimisation, among others.

Intensity-modulated radiotherapy requires generating treatment plans tailored to the patient's anatomy. Although inverse-planning methods are employed to automatically optimise treatment delivery parameters according to dosimetric objectives, achieving optimal plans still demands substantial intervention from the planner. The process can be resource-demanding and result in treatment plan quality variability among different users/experts [4]. Several standardised class solutions, i.e., planning solutions templates, have been proposed for targets presenting similar geometry and anatomical location [5,6]. These solutions are designed based on clinical expertise and knowledge from previous successful treatment plans and can be updated and improved based on new clinical insights. The use of templates may make the treatment planning (TP) process more streamlined and efficient, enabling clinicians to focus more on patient care. It also leads to more reliable and reproducible treatment plans, ensuring that the same quality standards are maintained across different cases and reducing the potential for human error and variability [4–7]. However, benchmarking and validation of automated planning are not straightforward, requiring expert physics resources. Most literature assesses treatment plans using dose volume histograms (DVHs) metrics for planning target volume (PTV) and organs at risk (OAR), as well as DVHs-derived metrics like conformity index (CI), homogeneity index (HI), tumour control probability (TCP), and normal tissue complication probability (NTCP) [7]. On the other hand, the individual characterisation of the patient and tumour plays a key role in treating the tumour with radiation alongside the interaction with other therapeutic modalities [8]. Molecular imaging may facilitate the customised biologically-guided dose painting (BGDP) strategy to be delivered by means of IMRT [9]. For a wide range of biological processes, modern positron emission tomography (PET) imaging offers cross-sectional data of the metabolism of a dedicated radiotracer injected in the patient; it provides high-resolution imaging with high sensitivity and specificity [10]. These non-invasive image modalities are currently used as tools for diagnosis and follow-up of treatment response, and even more, they may be used for prognosis and as a therapeutic tool for identifying areas of poor response [11,12].

This work presents a BGDP strategy within an automated TP pipeline. The information extracted from hypoxia-PET and [18F]fluorodeoxyglucose (FDG)-PET images is synergistically combined pre-optimisation to drive a dose prescription strategy and post-optimisation to assess the radiobiological response. This workflow aims at identifying failure-prone sub-volumes to be monitored and targeted within an adaptive radiotherapy (ART) framework.

Materials and methods

The ART framework presented in this paper consists of an automated TP workflow based on functional imaging. The framework is assisted *via* scripting in RayStation TP System (research version 10B-R) installed on a 64-bit Windows workstation computer with two Intel® Xeon® 3.4 GHz processors and 128 GB DDR4 RAM.

CONTACT Ana Ureba ana.ureba@ki.se Department of Physics, Medical Radiation Physics, Stockholms Universitet, Stockholm, Sweden; ;Department of Oncology-Pathology, Medical Radiation Physics, Karolinska Institutet, Stockholm, Sweden

Supplemental data for this article can be accessed online at https://doi.org/10.1080/0284186X.2023.2249221.

The automated pipeline consisted of three steps, as follows (Figure 1):

1. Dose prescription derived from PET images:
   Calculation of the prescribed dose distribution to be delivered as BGDP accounting for the radiosensitivity due to the partial pressure of oxygen (pO_2) and the clonogenic cell number (CCN) distributions and aiming at 95% TCP in the clinical target volume (CTV) [13,14]. FDG-PET is used for characterising the tumour cell density accounting for the heterogeneous cell distribution within the tumour [15]. FMISO-PET is used for identifying hypoxic regions providing quantitative information on the heterogeneous oxygenation level of the tumour. The combination of both PET modalities enables the identification of radio-resistant areas (such as hypoxic volumes) and it facilitates the precise prescription of the required radiation dose for effective tumour control.
2. Plan optimisation:
   a. Pre-optimisation: algebra combinations of the volumes of interest based on a template (more details in the supplementary material). Due to the challenging proximity and intersection of OARs with the targets, auxiliary structures were created aiming for controlling demanding dose gradients, steep dose fall-off, and avoiding overlapping volumes.
   b. The whole optimisation process was composed of three different steps:
      i. an optimisation where targets were prioritised and the spinal cord and brain stem were considered as avoidable volumes;
      ii. optimisation of the previous solution for reducing the dose to OARs to meet the clinical dose constraints;
      iii. minimax optimisations that mimicked at voxel level both the OAR doses retrieved from (ii) for doses below dose constraint and the prescribed doses to the targets. New objective functions were created at the beginning of this optimisation step. After each optimisation, if PTV coverage was not fulfilled, the weight of the OAR's objective function with the highest value was automatically decreased (Table 1).
3. Treatment plan dosimetric and radiobiological evaluation:
   a. Dose metrics of the nominal plan were scored: D_{mean}, $D_{95\%}$, $D_{2\%}$, for target volumes; the CI and HI, accounting for target coverage and homogeneity [16,17]; D_{mean}, $D_{2\%}$ accounting for OAR dose constraints; and NTCP after planning.
   b. pO_2 and CCN maps derived in step 1 were loaded in RayStation as beamsets and used as the underlying information for calculating TCP after planning. Local oxygen changes at voxel level over the course of the treatment due to changes in acute hypoxia were considered and simulated by resampling the pO_2 values within each target volume as previously proposed [18]. The results are reported in terms of equivalent dose in 2 Gy fractions (EQD2) for a more

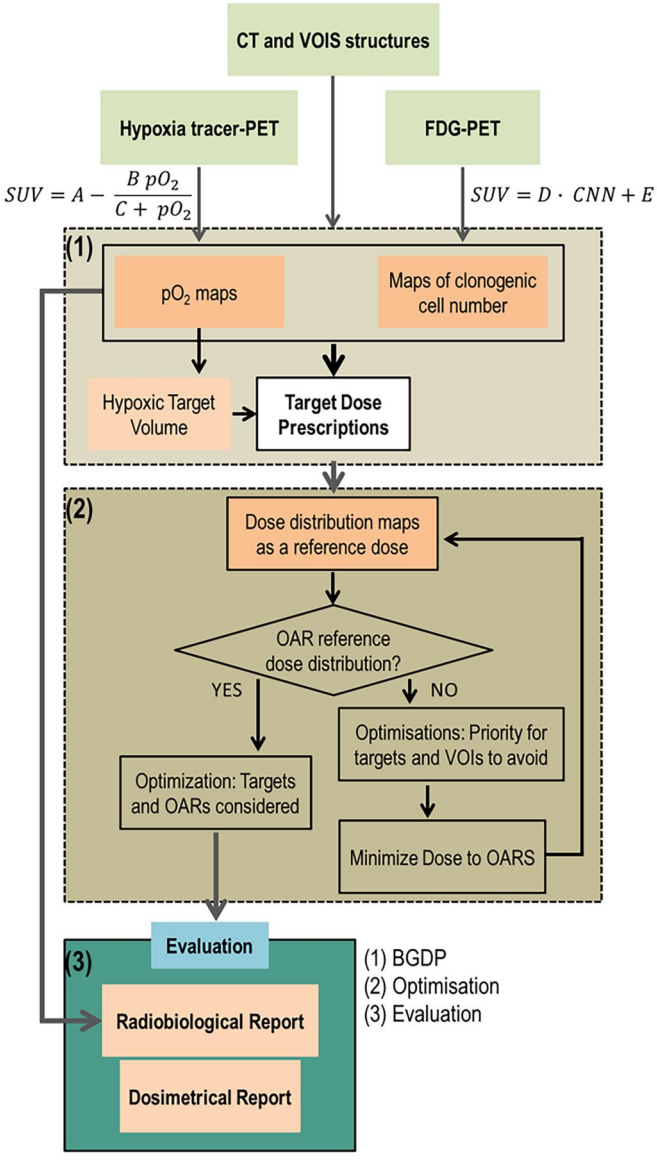

Figure 1. Automated planning workflow.

Table 1. OAR desired clinical dose and acceptance criteria.

	Priority	Clinical goal type	Volume	Acceptance criteria (Gy)
Spinal cord	1	Dose at volume	2%	50
Mandible	4	Dose at volume	2%	75
Brain stem	1	Dose at volume	2%	60
Parotids	4	Average dose (single gland)		20
		Average dose (at least one gland)		30
Oesophagus	4	Average dose		55
		Dose at absolute volume	0.03 ml	60
Cochlea	4	Dose at volume	2%	55

comprehensive comparison among different patients. Aiming to identify failure-prone sub-volumes, the spatial distribution of the number of survival cells (SCN) at the voxel level was reported based on the linear quadratic (LQ) model [19], failing voxels were coded to distinguish which was the failing target (Table 2).

The starting priorities and/or penalty factor parameters were predefined as part of the class solution. However, the optimisations in (i) and (iii) were repeated until no further improvement was possible. Triggered adaptation of the treatment is enabled by providing the size and the location of the sub-volumes in which the treatment is expected to fail with respect to the probability of controlling the tumour cells. The definition of the triggering parameters in terms of treatment adaptation is not automated but left to the choice of the user as the treatment adaptation is considered to be a clinical decision taken on individual bases. The automated pipeline could be repeatedly employed as many times as the imaging information is available during the course of the treatment.

The results of the presented workflow are illustrated for two selected head and neck cancer patients that were imaged with FMISO- and FDG-PET. Detailed information about the clinical and demographic characteristics of the cohort, including the patients selected for the illustration of the workflow, is given in Lazzeroni et al. [12]. Rigid co-registration of each PET image set with the planning CT was performed by using the registration module available in RayStation TPS. Photon beam plans were obtained using linear accelerator TrueBeam STx from Varian (Varian, Palo Alto, CA) to optimise two full arcs VMAT 6 MV (collimator angles 15° and 345°). Four target volumes were considered for planning: the PTV, the CTV, the gross tumour volume (GTV), and the hypoxic tumour volume (HTV). PTV had a fixed dose prescription of 52.5 Gy for all the cases.

Table 2. TCP parameter values.

Parameter	Value
n	35
α	0.32 Gy^{-1}
α/β	10 Gy
TCP	0.95

Results

Prior to planning, HTV was segmented by thresholding pO_2 values lower than 10 mmHg and biologically guided prescription dose distributions aiming at 95% TCP in the CTV were generated (Figure 1). Homogenous dose levels were prescribed to the CTV-GTV, GTV-HTV, and HTV. For the two presented examples in Figures 1 and 2, the prescribed dose were ranging from 68.2 to 71 Gy for CTV-GTV, 71.9 Gy to 75.6 Gy for GTV-HTV, and 78.0 to 83.5 Gy for HTV, respectively. Then, treatment plans with an integrated boost were automatically generated (Figure 2).

Post-optimisation plan evaluation was conducted using DVH metrics, focusing on aspects such as target coverage, OAR dose metrics (D_{mean}, $D_{2\%}$), and NTCP values. However, for assessing the radiobiological response, the actual TCP was calculated by leveraging the biological information

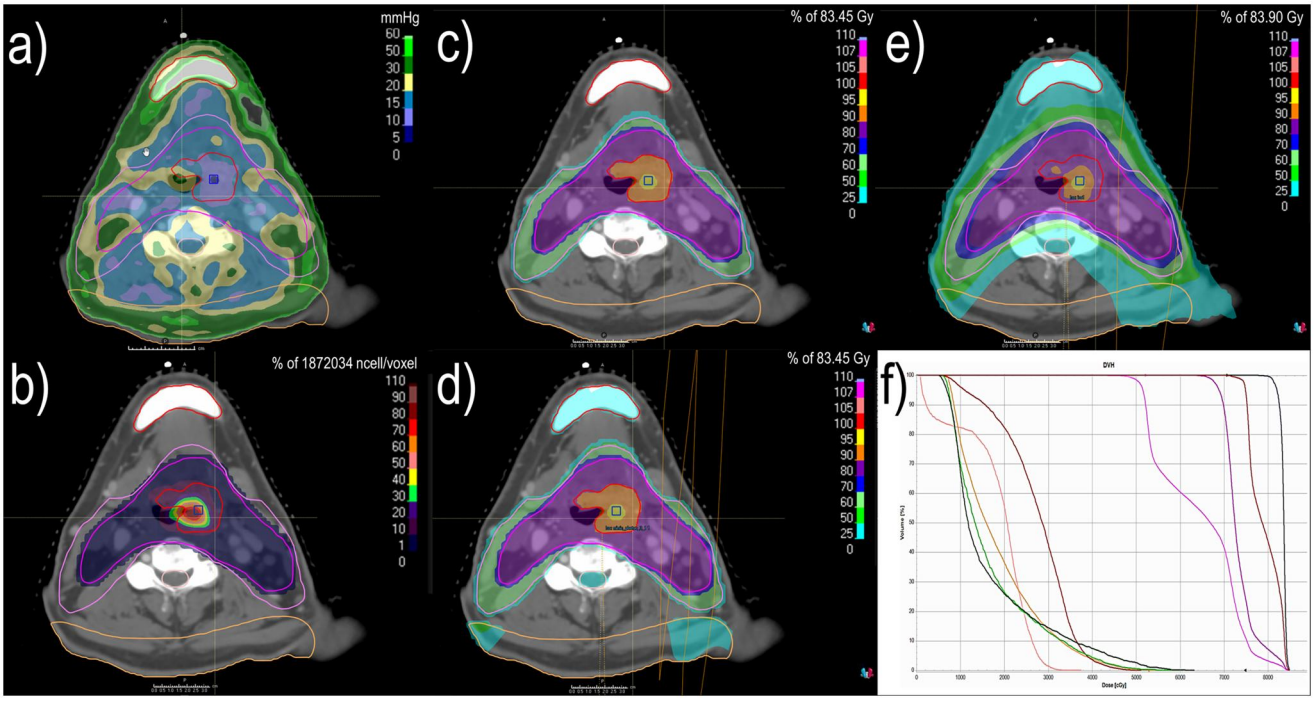

Figure 2. Axial view corresponding to (a) pO_2 distribution derived from FMISO-PET, (b) number of clonogenic cells per voxel derived from FDG-PET, (c) prescription dose to targets, (d) dose map to be mimicked, (e) planned dose distribution, and (f) DVHs. In solid lines, the volumes of interest: PTV, CTV, GTV, and HTV are light pink, dark pink, red, and dark blue, respectively; mandible, neck, parotid glands, and spinal cord are red, orange, light green, and light pink.

obtained from PET images. Since TCP represents a single value and does not provide spatial information, the identification of sub-volumes prone to treatment failure was based on the three-dimensional (3D) distributions of EQD2 and the SCN estimated by incorporating radiosensitivity derived from both FDG- and FMISO-PET images (Table 3).

Figure 3 shows an example of a treatment plan having a TCP of 92% in the CTV. Despite fulfilling the target clinical goals and target dose prescriptions and having the parotids well spared, the control of the tumour is lost due to a small volume at the periphery of the CTV close to one of the parotid glands.

Discussion

In recent years, there has been a growing emphasis on optimising radiation delivery in terms of technology. This emphasis includes improving the accuracy of tumour targeting, refining dose calculations, advancing imaging techniques for TP, and utilising advanced delivery methods such as IMRT, image-guided radiotherapy, or IMPT [20]. BGDP is intricately linked to ART and holds the potential to enhance decision-making processes for improving tumour control and sparing OAR. Despite the correlation between biological changes during treatment and clinical outcome [21], the clinical implementation of biologically guided ART remains largely limited to a few clinical trials investigating subvolume boosting and dose scheme modifications based on functional imaging [21,22]. However, there is still a need for further development of strategies and methods for effectively incorporating functional data in ART [21]. The presented strategy outlines a method for integrating functional information into the TP workflow. In our framework, the first and third steps of the TP process necessitate functional information as input. Consequently, if a new functional image becomes available during the treatment course, a revised prescription dose distribution can be calculated using step 1. After image registration of the new CT/PET with the original planning CT, it becomes possible, in step 3, to evaluate the TCP maps based on the initially planned dose distribution using the newly acquired functional image data.

It is evident that the BGDP approach presented here, incorporating functional information during TP, is likely to enhance the probability of achieving tumour control when compared to the non-BGDP strategy, especially in cases where an additional boost based on functional information is required. The prescribed doses, tailored to the biological properties of the tumour, contribute to a higher TCP in comparison to a non-BGDP approach. Furthermore, while prioritising tumour control, BGDP also allows for dose escalation/de-escalation to the tumour while maintaining acceptable OAR doses. The integration of functional information during mid-treatment enables adaptive planning, facilitating adjustments to treatment strategies in response to observed changes during the course of treatment, such as volumes failing TCP.

The tools presented in this study will help in the decision-making process of ART. However, it is essential to consider the limitations and challenges associated with image registration accuracy, functional image uncertainties, and the complexity of radiobiological models, which may influence the results.

The evaluation tools developed in the presented automated TP pipeline for BGDP enable the identification of subvolumes that are more likely to be prone to treatment failure and could thus be targeted in an ART strategy.

Table 3. Parameters used for NTCP calculation for selected OARs.

OAR name	TD50 (Gy)	n	m	α/β (Gy)	End point
Spinal cord	66.5	0.05	0.175	3	Myelopathy
Parotids	46	0.7	0.18	3	Xerostomia
Mandible	72	0.07	0.1	3.5	Osteoradionecrosis
Brain stem	65	0.16	0.14	2	Necrosis

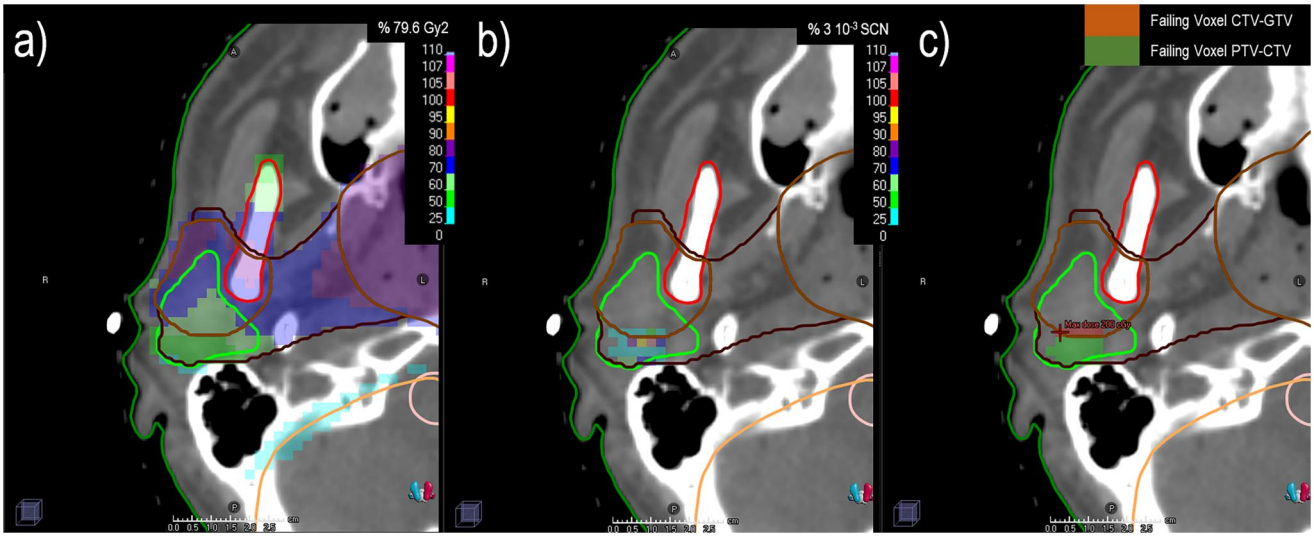

Figure 3. Axial view corresponding to (a) EQD2 of the planned physical doses, (b) surviving cell number distribution after 35 fractions, and (c) marked voxels with failing control. In solid lines, the volumes of interest: patient body contour, PTV and CTV are green, dark brown, and brown, respectively; mandible, neck, parotids, and spinal cord are red, orange, light green, and light pink.

Acknowledgements

Financial support from the Cancer Research Funds of Radiumhemmet, the Swedish Cancer Society and the Swedish Research Council (2020-04618) is gratefully acknowledged.

Disclosure statement

No potential conflict of interest was reported by the author(s).

Funding

Financial support from the Cancer Research Funds of Radiumhemmet, The Swedish Cancer Society, and The Swedish Research Council (2020-04618) is gratefully acknowledged.

ORCID

Ana Ureba http://orcid.org/0000-0002-1099-733X
Iuliana Toma-Dasu http://orcid.org/0000-0002-7101-240X
Marta Lazzeroni http://orcid.org/0000-0001-6676-508X

Data availability statement

The data that support the findings of this study are available from the corresponding author, AU, upon reasonable request.

References

[1] Hawkins PG, Kadam AS, Jackson WC, et al. Organ-sparing in radiotherapy for head-and-neck cancer: improving quality of life. Semin Radiat Oncol. 2018;28(1):46–52. doi: 10.1016/j.semradonc.2017.08.002.

[2] Holt A, Van Gestel D, Arends MP, et al. Multi-institutional comparison of volumetric modulated arc therapy vs. intensity-modulated radiation therapy for head-and-neck cancer: a planning study. Radiat Oncol. 2013;8:26. doi: 10.1186/1748-717X-8-26.

[3] Choudhury A, Budgell G, MacKay R, et al. The future of image-guided radiotherapy. Clin Oncol (R Coll Radiol). 2017;29(10):662–666. doi: 10.1016/j.clon.2017.04.036.

[4] Nelms BE, Robinson G, Markham J, et al. Variation in external beam treatment plan quality: an inter-institutional study of planners and planning systems. Pract Radiat Oncol. 2012;2(4):296–305. doi: 10.1016/j.prro.2011.11.012.

[5] Cilla S, Deodato F, Romano C, et al. Personalized automation of treatment planning in head-neck cancer: a step forward for quality in radiation therapy? Phys Med. 2021;82:7–16. doi: 10.1016/j.ejmp.2020.12.015.

[6] Hazell I, Bzdusek K, Kumar P, et al. Automatic planning of head and neck treatment plans. J Appl Clin Med Phys. 2016;17(1):272–282. doi: 10.1120/jacmp.v17i1.5901.

[7] Hussein M, Heijmen BJ, Verellen D, et al. Automation in intensity modulated radiotherapy treatment planning—a review of recent innovations. Br J Radiol. 2018;91(1092):20180270. doi: 10.1259/bjr.20180270.

[8] Overgaard J, Aznar MC, Bacchus C, et al. Personalised radiation therapy taking both the tumour and patient into consideration. Radiother Oncol. 2022;166:A1–A5. doi: 10.1016/j.radonc.2022.01.010.

[9] Bonomo P, Merlotti A, Olmetto E, et al. What is the prognostic impact of FDG PET in locally advanced head and neck squamous cell carcinoma treated with concomitant chemo-radiotherapy? A systematic review and meta-analysis. Eur J Nucl Med Mol Imaging. 2018;45(12):2122–2138. doi: 10.1007/s00259-018-4065-5.

[10] Mankoff DA, Pantel AR, Viswanath V, et al. Advances in PET diagnostics for guiding targeted cancer therapy and studying in vivo cancer biology. Curr Pathobiol Rep. 2019;7(3):97–108. doi: 10.1007/s40139-019-00202-9.

[11] Lilburn DM, Groves AM. The role of PET in imaging of the tumour microenvironment and response to immunotherapy. Clin Radiol. 2021;76(10):784.e1–784.e15. doi: 10.1016/j.crad.2021.08.004.

[12] Lazzeroni M, Ureba A, Wiedenmann N, et al. Evolution of the hypoxic compartment on sequential oxygen partial pressure maps during radiochemotherapy in advanced head and neck cancer. Phys Imaging Radiat Oncol. 2021;17:100–105. doi: 10.1016/j.phro.2021.01.011.

[13] Toma-Dasu I, Uhrdin J, Antonovic L, et al. Dose prescription and treatment planning based on FMISO-PET hypoxia. Acta Oncol. 2012;51(2):222–230. doi: 10.3109/0284186X.2011.599815.

[14] Toma-Daşu I, Daşu A, Brahme A. Dose prescription and optimisation based on tumour hypoxia. Acta Oncol. 2009;48(8):1181–1192. doi: 10.3109/02841860903188643.

[15] Zhou SM, Wong TZ, Marks LB. Using FDG-PET activity as a surrogate for tumor cell density and its effect on equivalent uniform dose calculation. Med Phys. 2004;31(9):2577–2583. doi: 10.1118/1.1779372.

[16] Lomax A, Scheib SG. Quantifying the degree of conformity in radiosurgery treatment planning. Int J Radiat Oncol Biol Phys. 2003;55(5):1409–1419. doi: 10.1016/s0360-3016(02)04599-6.

[17] Wu Q, Mohan R, Morris M, et al. Simultaneous integrated boost intensity-modulated radiotherapy for locally advanced head-and-neck squamous cell carcinomas. I: dosimetric results. Int J Radiat Oncol Biol Phys. 2003;56(2):573–585. doi: 10.1016/s0360-3016(02)04617-5.

[18] Kjellsson-Lindblom E, Ureba A, Dasu A, et al. Impact of SBRT fractionation in hypoxia dose painting—accounting for heterogeneous and dynamic tumor oxygenation. Med Phys. 2019;46(5):2512–2521. doi: 10.1002/mp.13514.

[19] McMahon SJ. The linear quadratic model: usage, interpretation and challenges. Phys Med Biol. 2018;64(1):01TR01. doi: 10.1088/1361-6560/aaf26a.

[20] Stewart RD, Li XA. BGRT: biologically guided radiation therapy—the future is fast approaching! Med Phys. 2007;34(10):3739–3751. doi: 10.1118/1.2779861.

[21] Glide-Hurst CK, Lee P, Yock AD, et al. Adaptive radiation therapy (ART) strategies and technical considerations: a state of the ART review from NRG oncology. Int J Radiat Oncol Biol Phys. 2021;109(4):1054–1075. doi: 10.1016/j.ijrobp.2020.10.021.

[22] Matuszak MM, Kashani R, Green M, et al. Functional adaptation in radiation therapy. Semin Radiat Oncol. 2019;29(3):236–244. doi: 10.1016/j.semradonc.2019.02.006.